PERGAMON

International Journal of Multiphase Flow 26 (2000) 191–206

International Journal of Multiphase Flow

www.elsevier.com/locate/ijmulflow

Bubble transport in flashing flow

E. Elias [a,*], P.L. Chambré [b]

[a] *Faculty of Mechanical Engineering Technion, Haifa, Israel*
[b] *Department of Nuclear Engineering, University of California, Berkeley, CA 94720, USA*

Received 21 July 1998; received in revised form 13 February 1999

Abstract

A bubble transport equation, based on the theory of bubble nucleation and growth, is applied for the analysis of two-phase flashing flows. Spontaneous nucleation at the flashing inception point and heterogeneous nucleation in the liquid bulk are used as boundary and initial conditions, respectively. Analytical solution of the transport equation yields a constitutive relation for the net vapor generation rate along the tube, which is required for closure of a two-fluid set of conservation and balance equations. Model predictions, in terms of flow rates and void fraction distributions, compare favorably with measured data. A mechanistic representation of the thermodynamic and transport conditions at the flashing inception point is described. © 2000 Elsevier Science Ltd. All rights reserved.

1. Introduction

Flashing flows are encountered in a variety of industrial and geo-thermal processes, such as volcanic flow, two-phase flow in boilers and steam generators, flow of saturated and subcooled liquid in pipes and in converging-diverging nozzles, cryogenics and two-phase critical flow during a hypothetical loss of coolant accident in nuclear reactors (Elias and Lellouche, 1994). Flashing occurs when liquid is brought into a metastable state by intense heating or rapid depressurization. At a certain degree of superheat, a limit is reached (often termed 'flashing inception point') at which vapor is suddenly generated in an explosive manner. Vapor generation persists downstream of the flashing inception point at a lower rate as a result of heterogeneous nucleation and growth of existing bubbles. Realistic modeling of flashing flows must, therefore, consider both the instantaneous nucleation at the flashing inception point as

* Corresponding author.

0301-9322/00/$ - see front matter © 2000 Elsevier Science Ltd. All rights reserved.
PII: S0301-9322(99)00011-7

well as the continuously varying number density and size distribution of the bubble population further downstream.

The thermodynamic conditions at the flashing inception point have been rigorously studied, both theoretically (Alamgir and Lienhard, 1981; Saha et al., 1984; Skripov et al., 1988; Lee and Schrock, 1990; Elias and Chambré, 1993) and experimentally (Reocreux, 1974; Wu et al., 1981; Alamgir et al., 1981). The degree of superheat required for initiating nucleation has been shown to depend on the flow and surface conditions as well as on the rate of depressurization or heating. In slow transients, the degree of superheat at the onset of flashing may be considerably lower than the kinetic limit of nucleation. On the other hand, at higher heating or decompression rates, only some small fraction of the existing nucleation sites in the liquid is activated before the liquid superheat approaches the maximum nucleation limit. Thus, at extremely rapid transients the liquid superheat approaches the value determined by random density fluctuations that lead to homogeneous nucleation. These extreme situations are, however, rarely encountered in engineering processes. For a typical fluid flowing in a pipe the initial bubble formation is dominated by heterogeneous nucleation.

Vapor generation downstream of the flashing inception point is a relative slow process. In pipe flow (Reocreux, 1974), the fluid may accelerate for more than 100 ms before reaching critical conditions. At higher decompression rates, typical to flow in a converging-diverging nozzle (Wu et al., 1981), the nucleation zone could be much shorter. Several studies attempt to solve the heat and mass transfer phenomena in the nucleation zone downstream of the flashing inception point using a number of arbitrary parameters and assumptions to fit the experimental data. The most common approach is to neglect the nucleation downstream of the flashing point by assuming that the number density of bubble nuclei remains unchanged during the process (Wolfert, 1976; Edwards, 1968; Dagan et al., 1993). While simplifying the analysis and sometimes successfully predicts the critical mass flux, this assumption does not necessarily describe the correct physical conditions in the flow channel.

Riznic and Ishii (1989) suggested a differential balance equation for the size-integrated bubble number density. Size distribution was determined independently using an approximate integral relation of the bubble growth equation. Analysis of the bubble number density along the flow path was based on wall nucleation and neglected homogeneous and bulk heterogeneous nucleation. Yan (1991) using an eight-equation model to predict the flow parameters and the bubble density distribution in a critical flashing flow later studied these phenomena. The initial explosive generation of nuclei at the flashing inception point was determined by integrating the bubble equation from the point of saturation to the flashing point. A statistical approach was recently applied by Guido-Lavalle et al. (1994) and by Herrero et al. (1995) to derive a transport equation for non-condensable bubbles in gas–liquid flows. A distribution function was defined to represent the varying number density of bubbles of a given volume at a given position. The model accounts for bubble break-up and coalescence phenomena but neglects evaporation and condensation. In general, the use of a bubble transport equation in the analysis of non-equilibrium two-phase flow, extends previous models (e.g., Ardron, 1978) which considered only bubbles of uniform size.

The prime purpose of this work is to develop a mechanistic flashing model which accounts for both, non-equilibrium vapor generation at the flashing inception point and bulk heterogeneous nucleation along the flow path. The model is based on the bubble transport

equation derived by Elias & Chambré (1984) for determining the bubble number density, and utilizes a general correlation (Elias and Chambré, 1993) for computing the effect of heterogeneous nucleation. The thermodynamic conditions and the nucleation rate at the flashing point are used to define the necessary boundary conditions of the problem. Analytical solution of the bubble transport equation is combined as a constitutive relation with a two-fluid set of balance equations to predict the pressure and void fraction along a circular duct. Model predictions are validated against the experimental data of Reocreux (1974).

2. The bubble species equation

A mechanistic bubble species model has been derived in Elias and Chambré (1984). In the following, a consistent set of boundary and initial conditions is developed to enable the implementation of the resulting bubble equation in a two-fluid representation of flashing nonequilibrium two-phase flows.

To derive the bubble equation, we characterize a vapor–liquid flow by a concentration function, N, defined as the number of bubbles of radius r lying between r and $r+dr$, per unit volume of fluid and vapor mixture, per unit radius difference, dr. The number density of bubbles whose radii lie between r and $r+dr$ is, accordingly, Ndr.

Neglecting bubble coalescence and break-up, the number density of bubbles in a volume element bounded between z and $z+\Delta z$ and between r and $r+\Delta r$, is defined by two processes: bubble convection and bubble growth. Since in a steady-state, the rate of change in the total mass of bubbles in the volume must vanish, we get:

$$0 = A(z)\rho_G(z)\Delta z\left\{\left(N\frac{Dr}{Dt}\right)\bigg|_{z,r} - \left(N\frac{Dr}{Dt}\right)\bigg|_{z,r+\Delta r}\right\} + \Delta r\{(A\rho_G u_G N)\,|_{z,r} - (A\rho_G u_G N)\,|_{z+\Delta z,r}\} \quad (1)$$

where Dr/Dt is a substantial derivative, A is flow area, ρ density, u velocity and the subscript G refers to the vapor phase. The first terms on the RHS of Eq. (1) describes the growth rate of bubbles into and out of the radius range r to $r+\Delta r$. The second term defines the convection rate of bubbles of radius r into the control volume through the face at z and out through the face at $z+\Delta z$. Dividing Eq. (1) by $\Delta z\Delta r$ and taking the limit as these dimensions approach zero, we get after some rearrangements:

$$0 = \frac{\partial}{\partial r}\left(N\frac{Dr}{Dt}\right) + \frac{1}{A(z)\rho_G(z)}\frac{\partial}{\partial z}[N(z,r)A(z)\rho_G(z)u_G(z)] \quad (2)$$

In a volume element which travels with the speed of the vapor, the bubble radius can be determined by (Forster and Zuber, 1954):

$$\frac{Dr}{Dt} = \beta^2(z,t)\frac{[T_L(z,t) - T_s(z,t)]^2}{r}, \quad \beta = \sqrt{\frac{3}{\pi}}\frac{\sqrt{(\lambda\rho C_p)_L}}{h_{LG}\,\rho_G} \quad (3)$$

where T_L is the temperature of the liquid surrounding the bubble, T_s is the vapor temperature

taken to be at saturation and h, λ, ρ and C_p denote enthalpy, conductivity, density and specific heat, respectively. The subscript L refers to the liquid phase. Denoting the initial radius of vapor nuclei as $r_o > 0$ and defining the new variables

$$n(z,\tau) = N(z,r)/r, \quad \beta_o = \beta(0), \quad \tau_o = \frac{1}{2}\left(\frac{r_o}{\beta_o T_s}\right)^2, \quad \tau = \frac{1}{2}\left(\frac{r}{\beta_o T_s}\right)^2 - \tau_o, \; \phi(z) = \left(1 - \frac{T_L(z)}{T_s(z)}\right)^2,$$

$$h(z) = \left[\frac{\beta(z)}{\beta_o}\right]^2 \frac{\phi(z)}{u_G(z)} \text{ and } g(z) = \frac{d}{dz} \ln[A(z)\rho_G(z)u_G(z)],$$

we get, after substituting Eq. (3) into Eq. (2):

$$h(z)\frac{\partial n(z,\tau)}{\partial \tau} + \frac{\partial n(z,\tau)}{\partial z} = -n(z,\tau)g(z) \tag{4}$$

Eq. (4) is a bubble species equation which describes the bubble number density and radii distribution, $n(z,\tau)$, along the channel. It is a first order nonhomogeneous hyperbolic equation which requires both 'initial' conditions at $\tau = 0$ and boundary conditions at $z = 0$, taken as the point of flashing inception.

2.1. Initial and boundary conditions

Along the flow channel, foreign bodies, dissolved gases and surface irregularities in the liquid bulk provide ample nuclei for vapor-bubble formation. Thus, the initial condition, $n(z,0)$, can be described as (Frenkel, 1955):

$$n(z,0) = n_2[1 - \epsilon(z)] \exp\left(-\frac{\psi \Delta G(z)}{3kT_L(z)}\right) \tag{5}$$

where ϵ is the local volumetric void fraction, ΔG is the Gibbs' free energy of formation of a critical vapor nucleus, k is Boltzmann's constant and n_2 is a constant describing the normalized number density of vapor nucleation sites in the liquid per unit radius difference.

Similar to the expression used in homogeneous nucleation of vapor bubbles (Hirth and Pound, 1963), the maximum free energy for vapor-bubble formation is:

$$\Delta G(z) = \frac{16\pi\sigma^3(z)}{\theta^2(z)p_s^2(z)[1 - \rho_G(z)/\rho_L(z)]^2} \tag{6}$$

in which σ is the liquid surface tension and $\theta \equiv (p_s(T_L) - p)/p_s(T_L)$ is a normalized difference between the local pressure, p, and the saturation pressure, p_s (T_L), corresponding to the liquid temperature.

The factor, ψ, in Eq. (5) is a dimensionless number between 0 and 1 which accounts for heterogeneous nucleation in the liquid volume. In Elias and Chambré (1993), ψ is formulated as a function of the liquid reduced temperature, T_r, and a dimensionless rate of depressurization, S:

$$\psi(z) = c_1 T_r^{c_2}(z) S^{c_3}(z) \tag{7}$$

where

$$S(z) = \frac{\Sigma(z)\rho_L(z)\sqrt{2\pi m k T_L(z)}}{16\pi\rho_G(z)\sigma^2(z)}, \quad \Sigma(z) = u_L(z)\frac{dp(z)}{dz} \tag{8}$$

and m is the mass of a liquid molecule.

The coefficients c_1 to c_3 in Eq. (7) were estimated by a least squares fit to a wide range of experimental data as: $c_1 = 1506.1$, $c_2 = 31.906$ and $c_3 = 0.310$. Note that Eq. (7) exhibits the physically correct trend of parameters in that ψ approaches zero at very low rates of depressurization (since $c_3 > 0$) and ψ increases with S.

The exact value of n_2 in Eq. (5) may depend on the local pressure and flow rate. However, for the range of conditions studied in two-phase critical flow experiments, the effect of n_2 on the predicted mass flux and void fraction was found to be small (Minzer, 1995). For the conditions studied by Reocreux (1974), increasing n_2 by a factor of 50 reduces the predicted mass flux by less than 5%. n_2 was taken, therefore, as constant ($n_2 = 10^{22}$ m^{-5}) in this study.

The boundary condition of Eq. (4), $n(0,\tau)$, represents the bubbles generated at the flashing point. Its derivation requires an independent estimation of the thermal hydraulic conditions at the flashing inception point ($z = 0$). At that point we consider a population of bubbles with uniformly distributed normalized radii in the range of 0 to τ_1 (maximum radius, r_1), such that:

$$n(0,\tau) = n_1\{U(\tau) - U(\tau - \tau_1)\} \tag{9}$$

where $U(\tau)$ is the unit step function. To determine n_1 and τ_1 one can equate the total rate of nucleation, I, in a small section of the flow channel, Δz, to the rate of nuclei removal by convection. Thus:

$$I\Delta z = \int_0^{r_1} n_1 r u_L(0) dr \tag{10}$$

The radius, r_1, in a temperature field which varies between an initial value, $T_L(0)$, and the saturation temperature corresponding to the minimum pressure at the flashing inception point, $T_s(p_m)$, was derived by Olek et al. (1990) as:

$$r_1 = \frac{2\beta}{3}[T_L(0) - T_s(p_m)]\sqrt{t_m}, \tag{11}$$

where t_m is the time required for a nuclei to reach a departure radius, r_1.

Assuming the normalized density, n_1, to be independent of r and using $\Delta z = t_m u_L$, we obtain upon integration of Eq. (10):[1]

$$n_1 = \frac{9}{2}\frac{I}{\beta^2[T_L(0) - T_s(p_m)]^2} \tag{12}$$

[1] The authors are indebted to the reviewer for suggesting this form of n_1.

The flashing inception pressure, p_m, can be determined following Elias and Chambré (1993) where the dimensionless pressure, $\theta_m \equiv (p_s(T_L) - p_m)/p_s(T_L)$, is determined as a solution of the transcendental equation:

$$\left(\frac{4\Sigma(0)}{\sqrt{\pi}p_s}\right)^4 \frac{1}{3\delta v_b}\left(\frac{\Delta G_m}{kT_L A(\theta_m)\theta_m}\right)^3 = \frac{I}{\psi^3} \tag{13}$$

where v_b is the volume of a vapor molecule and δ and $A(\theta_m)$ are dimensionless functions defined at the flashing inception point as:

$$\delta \equiv \frac{a_h \rho_G h_{lg} + \rho_L(\rho_L - \rho_G)}{p_s(a_h + a_p \rho_L)},$$

$$A(\theta_m) \equiv \left(\frac{3v_b}{4\pi}\right)^{2/3} \frac{4\pi\rho_G p_s \theta_m}{\rho_L\sqrt{2\pi m k T_L}}$$

The thermodynamic derivatives, a_h and a_p are:

$$a_h \equiv \left(\frac{\partial \rho_L}{\partial h_L}\right)_{p_L}, \quad a_p \equiv \left(\frac{\partial \rho_L}{\partial p_L}\right)_{h_L}$$

The rate of heterogeneous nucleation per unit volume of liquid at the flashing inception point, I, can be calculated by the Zeldovich–Kagan theory (Skripov et al., 1988):

$$I = N'\sqrt{\frac{2\sigma}{\pi m B}} \exp\left(-\frac{\psi \Delta G_m}{3kT_L}\right) \tag{14}$$

where N' is the number density of the liquid molecules, $B \approx 1$ is the cavitation factor (Blander, 1979) and the maximum free energy, ΔG_m, is defined in terms of θ_m (Eq. (6)).

2.2. Solution of the bubble species equation

Solution of Eq. (4) by the Laplace transform method was derived by Elias and Chambré (1984). The solution yields the bubble population, $n(z,\tau)$, as a sum of two groups: bubbles generated at the flashing point, $n_1(z,\tau)$, and bubbles generated along the flow path downstream of the flashing point, $n_2(z,\tau)$. The first group is given by:

$$n_1(z,\tau) = n_1 \frac{m(0)}{m(z)}\{U[\tau - a(z)] - U[\tau - (\tau_1 + a(z))]\} \tag{15}$$

where

$$a(z) = \int_0^z h(z')\mathrm{d}z', \quad m(z) = A(z)u_G(z) \tag{16}$$

Eq. (15) represents a positive pulse of magnitude $n_1 m(0)/m(z)$ and duration $a(z) < \tau < (\tau_1 + a(z))$.

The second group is given by:

$$n_2(z,\tau) = \frac{m(z')}{m(z)} n(z',0), \quad 0 < \tau < a(z)$$

$$n_2(z,\tau) = 0, \ \tau > a(z) \tag{17}$$

where z' indicates the location at which the vapor-bubble was originated, given by the explicit solution of

$$a(z') = a(z) - \tau \tag{18}$$

Fig. 1 illustrates schematically the parameters affecting the solution. The bubble size parameter, τ, is plotted vs the distance from the point of flashing inception ($z = 0$). Bubbles with radii in the range of 0 to r_1 are generated locally at the flashing inception point. In addition, new bubbles of radius corresponding to $\tau = 0$ are continuously introduced along the channel. At a given position, downstream of the flashing point, the total number density function consists of two populations, $n_1(z,\tau)$ and $n_2(z,\tau)$. Hence, the solution has a discontinuity at $\tau = a(z)$, representing the maximum size of $n_2(z,\tau)$, as noticed from Eq. (17). There are no bubbles larger than the limit $\tau_1 + a(z)$, representing the size at z of a vapor bubble created at the flashing inception point with dimensionless radius τ_1.

In the following Eqs. (15) and (17) are used to derive a vapor generation term.

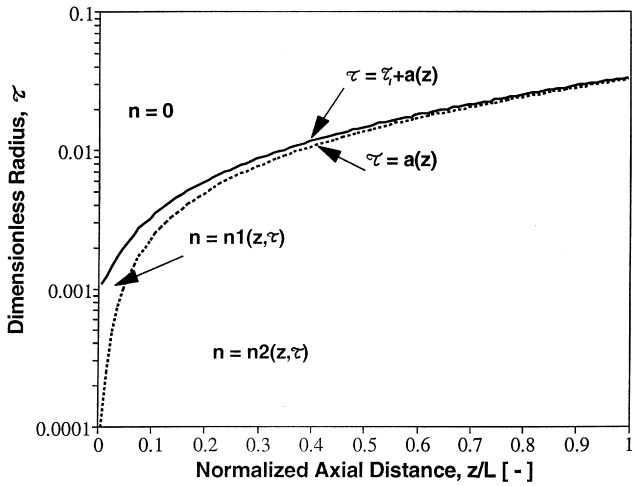

Fig. 1. Bubble population along flow path.

2.3. Vapor generation in flashing flow

A vapor source term, Γ, can be readily derived by integrating the growth rate of all the bubbles present at a given position in the liquid. This procedure yields (Elias and Chambré, 1984):

$$\Gamma = \frac{F(z)}{m(z)}\left\{\frac{3}{2}\int_z^0 n(z',0)m(z')\sqrt{a(z)-a(z')}h(z')\mathrm{d}z' + n_1 m(0)[(\tau_1 + a(z))^{3/2} - a(z)^{3/2}]\right\} \tag{19}$$

where

$$F(z) = \frac{8\sqrt{2}}{3}\pi[\beta(z)T_s(z)]^5 A(z)\rho_G(z)u_G(z)\phi(z). \tag{20}$$

Thus, for a given liquid pressure and temperature one can determine $n(z',0)$ from Eq. (5), $a(z)$ and $m(z)$ from Eq. (16) and solve Eq. (19) for the rate of vapor generation at point z in the flow channel. A more convenient form of Eq. (19) is obtained by approximating the integrand using a first order Taylor series, to yield:

$$\Gamma = \frac{F(z)}{m(z)}\left\{\frac{3}{2}\sqrt{a(z)}\int_z^0 n(z',0)m(z')h(z')\mathrm{d}z' - \frac{3}{2\sqrt{a(z)}}\int_z^0 n(z',0)m(z')a(z')h(z')\mathrm{d}z' + n_1 m(0)[(\tau_1 + a(z))^{3/2} - a(z)^{3/2}]\right\}. \tag{21}$$

Eq. (21) was used as a constitutive relation in the following two-fluid model to predict the spatial distribution of fluid conditions in critical two-phase flow.

3. Two-fluid model formulation

Upstream of the flashing inception point the standard single-phase mass, momentum and energy equations are used. Beyond incipient flashing, the two-fluid conservation equations derived by Ishii (1975) are considered. To simplify the analysis we consider a steady-state, adiabatic and one-dimensional flow. The equations are averaged across the channel area by assuming that the pressure and temperature across any section normal to the flow are constant. Furthermore, by considering the vapor to be saturated with respect to the local pressure, the flow can be fully described by five conservation equations—two mass, two momentum and one energy:

Conservation of mass

$$\frac{\mathrm{d}}{\mathrm{d}z}(A\rho_k u_k \epsilon_k) = \Gamma_k \tag{22}$$

Conservation of momentum

$$\frac{1}{A}\frac{\mathrm{d}}{\mathrm{d}z}(A\rho_k\epsilon_k u_k^2) = -\alpha_k\frac{\mathrm{d}p}{\mathrm{d}z} - g\rho_k\epsilon_k\cos\ \Theta + \frac{\Gamma_k}{A}[\eta u_\mathrm{L} + (1-\eta)u_\mathrm{G}] + M_k - F_k \tag{23}$$

Conservation of mixture energy

$$A\epsilon\rho_\mathrm{G}u_\mathrm{G}^2\frac{\mathrm{d}u_\mathrm{G}}{\mathrm{d}z} + A(1-\alpha)\rho_\mathrm{L}u_\mathrm{L}^2\frac{\mathrm{d}u_\mathrm{L}}{\mathrm{d}z} + A(1-\epsilon)\rho_\mathrm{L}u_\mathrm{L}\frac{\mathrm{d}h_\mathrm{L}}{\mathrm{d}z} + A\epsilon\rho_\mathrm{G}u_\mathrm{G}\frac{\mathrm{d}h_\mathrm{G}}{\mathrm{d}p}\frac{\mathrm{d}p}{\mathrm{d}z}$$

$$= [h_\mathrm{lg} + \frac{1}{2}(u_\mathrm{G}^2 - u_\mathrm{L}^2)]\Gamma + Ag\ \cos\Theta[\rho_\mathrm{G}\epsilon u_\mathrm{G} + \rho_\mathrm{L}(1-\epsilon)u_\mathrm{L}] \tag{24}$$

where u, p, ρ and A denote respectively the velocity, pressure, density, and cross section area at axial position z in the duct. The subscript k denotes either the gas (k = G) or the liquid (k = L) phase, ϵ is the volumetric vapor concentration with $\epsilon_\mathrm{G} = \epsilon$ and $\epsilon_\mathrm{L} = 1-\epsilon$, and Γ_k is the rate of increase of the phase mass per unit length due to phase change such that $\Gamma_\mathrm{G} = \Gamma$ and $\Gamma_\mathrm{L} = -\Gamma$ as given in Eq. (21).

Before Eqs. (22)–(24) can be integrated, constitutive relations are required to define the interfacial conditions and the rate of interface mass and momentum transfer. Since the gas phase is assumed to be dispersed within the liquid phase, the wall shear stress on the gas phase is neglected, $F_\mathrm{G} = 0$. The liquid phase wall shear stress is:

$$F_\mathrm{L} = \frac{1}{2}\frac{f}{D}\rho_\mathrm{L}u_\mathrm{L} \mid u_\mathrm{L} \mid \tag{25}$$

where D is the channel diameter. For turbulent flow ($Re > 4000$) the friction factor, f, is modeled in Cheremisinoff and Gupta (1983) as:

$$\frac{1}{\sqrt{f}} = 1.14 - 2\ \log_{10}\left(\frac{\varepsilon}{D} + \frac{9.35}{Re\sqrt{f}}\right) \tag{26}$$

In the analysis of Reocreux (1974) data, a roughness coefficient, $\varepsilon = 5 \times 10^{-9}$ m was found to yield good predictions of the pressure distribution in the single-phase section of the channel. The flow Reynolds number in Eq. (26) is defined by the total mass flux, G, and the liquid viscosity, μ_L, as:

$$Re = \frac{GD}{\mu_\mathrm{L}} \tag{27}$$

The momentum transfer between the gas and liquid phases in Eq. (23) consists of two forces per unit volume:

$$M_\mathrm{L} = -M_\mathrm{G} = \epsilon(F_\mathrm{D} + F_\mathrm{VM}) \tag{28}$$

For bubbly flow ($\epsilon < 0.2$) the interfacial drag force, F_D, can be modeled as:

$$F_\mathrm{D} = \frac{3}{8}\rho_\mathrm{L}\frac{C_\mathrm{D}}{\bar{r}}(u_\mathrm{G} - u_\mathrm{L}) \mid u_\mathrm{G} - u_\mathrm{L} \mid \tag{29}$$

where the drag efficient, C_D, is given by Harmathy (1960) as:

$$C_D = \frac{4}{3}\bar{r}\left[\frac{g(\rho_L - \rho_G)}{\sigma(1-\epsilon)}\right]^{1/2} \tag{30}$$

For annular flow ($\epsilon > 0.9$), F_D is (Wallis, 1969):

$$F_D = \frac{2C_a}{D\sqrt{\pi}}\rho_G(u_G - u_L) \mid u_G - u_L \mid \tag{31}$$

where the interfacial friction coefficient, C_a, is (Wallis, 1969):

$$C_a = 0.079 Re_G^{-1/4}[1 + 75(1-\epsilon)] \tag{32}$$

The vapor Reynolds number, Re_G, is defined as:

$$Re_G = \frac{\rho_G D \epsilon u_G}{\mu_G} \tag{33}$$

For churn-turbulent flow ($0.2 < \epsilon < 0.9$) F_D is determined as a void weighted average value between the prediction of Eq. (29) at $\epsilon = 0.2$ and the prediction of Eq. (31) at $\epsilon = 0.9$.

The variable, $\bar{r}$, in Eq. (30) denotes the average radius of the bubble population,

$$\bar{r} = \left(\frac{3\epsilon}{4\pi N_t}\right) \tag{34}$$

The total bubble number density, N_t, can be obtained by direct integration over the bubble radii of n_1 from Eq. (15) and n_2 from Eq. (17). However, considering the functional relation between τ and z' in Eqs. (16) and (18), the integration can be conveniently performed over z:

$$N_t = n_1\frac{r_1^2}{2} + \frac{(\beta T_s)^2}{m(z)}\int_0^z m(z')n(z',0)h(z')\mathrm{d}z' \tag{35}$$

The virtual mass force, F_{VM} in Eq. (28), is considered only in the bubbly flow regime (Ruggles et al., 1989):

$$F_{VM} = \rho_L C_{VM}\left[u_G\frac{\mathrm{d}u_G}{\mathrm{d}z} - u_L\frac{\mathrm{d}u_L}{\mathrm{d}z}\right] \tag{36}$$

where the virtual volume coefficient, C_{VM}, is expressed as a function of the void fraction as:

$$C_{VM} = 0.5(1 + 12\epsilon^2) \tag{37}$$

The term containing η in Eq. (23) represents the effect of evaporative momentum transfer. Based on entropy production consideration (Wallis, 1969), $\eta = 1/2$ is used in this work, implying that the effective velocity of the evaporated liquid is $(u_G + u_L)/2$. The inclination angle of the flow channel is measured such that for horizontal flow $\cos\Theta = 0$ and for vertical upflow $\cos\Theta = 1$.

4. Results and discussion

The set of conservation equations was integrated numerically. For given flow rate and inlet pressure and liquid temperature, the single-phase steady-state equations were integrated along the flow channel until the fluid reached the flashing inception superheat, θ_m, determined by Eq. (13). Downstream of the flashing inception point the set of two-phase Eqs. (22)–(24), was solved subject to the inlet conditions and using the vapor generation rate, Eq. (21) and the set of constitutive relations Eqs. (25) to (37). These were supplemented by the specific system geometry and tables of thermodynamic and transport properties of water and vapor. The integrals in Eqs. (16), (21) and (35) were considered as three fictitious state variables,

$$y_1 = \int_0^z h(z')\mathrm{d}z' \tag{38}$$

$$y_2 = \int_0^z m(z')n(z',0)h(z')\mathrm{d}z' \tag{39}$$

$$y_3 = \int_0^z n(z',0)m(z')a(z')h(z')\mathrm{d}z' \tag{40}$$

Eqs. (22)–(24) and (38)–(40) constitute a set of eight coupled ordinary nonlinear first-order differential equations for the eight variables: p, ϵ, u_L, u_G, T_L, y_1, y_2 and y_3. The set of equations was integrated by a variable step Runge–Kutta procedure to yield the flow conditions along the flow channel on the basis of a global error specification. This method is particularly efficient for the solution of the present stiff equations.

The solution of the problem consists of setting up of an algorithm for the calculation of the flow parameters of the two phases along the test section for a given pair of inlet pressure and temperature. To predict the critical flow rate we employ the methodology suggested by Lemonnier and Selmer-Olsen (1992). It consists of postulating an inlet mass flux and tracking the changing flow conditions along the pipe starting from the given inlet conditions. Depending on the postulated mass flux one can obtain two main families of solution curves of physical interest. At lower mass flux (smaller than the critical flow rate), a subcritical flow pattern prevails and the numerical integration can be pursued up to the exit. Any flow rate larger than the critical flow rate does not yield a valid flow pattern, and the integration cannot be carried out beyond a point located upstream of the critical section. In practice the critical flow rate can be approached numerically within a given precision. When a diffuser section exists at the exit of a straight pipe, the flow becomes sonic in the straight section of the pipe and supersonic downstream. The choking point may occur anywhere along the diverging section. Thus, the numerical procedure concentrates basically on searching an inlet mass flux for which the solution represents a choked flow.

The model has been applied to predict the steady-state flashing experiments conducted by Reocreux (1974) in a circular vertical channel consisting of two parts; a lower stainless steel tube with an internal diameter of 20 mm and length of 2160 mm, and an upper diffuser section with an opening angle of 7° and a length of 327 mm leading to a cylindrical exit section with a

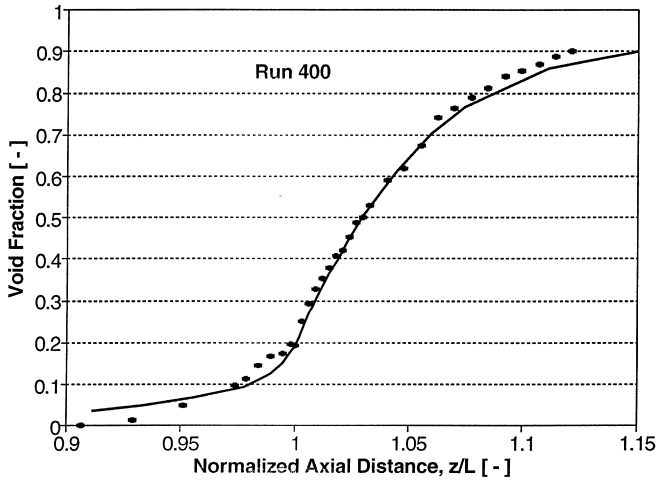

Fig. 2. Comparison with Reocreux's test 400.

diameter of 60 mm. Tests were conducted by introducing subcooled water at low pressures (0.21–0.34 MPa) to the bottom of the test section (at a physical elevation of −1.044 m). Pressure and area-averaged void fractions were measured along the flow channel.

The predicted critical mass flux were within ±3% of the measured data over the range of conditions reported in Reocreux (1974). Figs. 2–7 show typical results of void fraction distributions predicted by the present model in comparison with Reocreux's experimental data. The length coordinate was normalized such that the diffuser throat is at $z/L = 1$ and the test

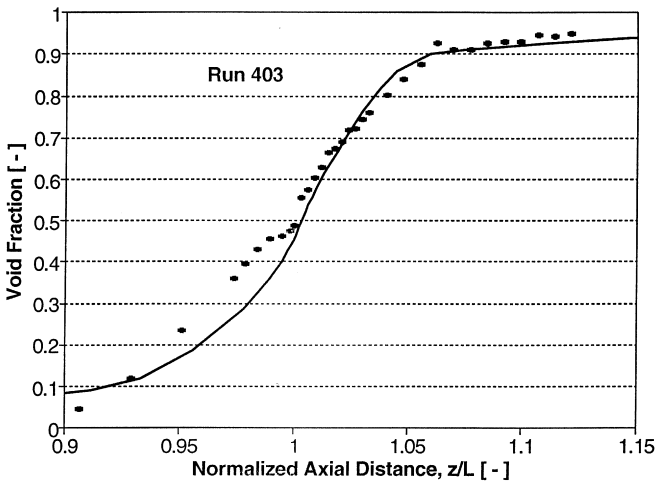

Fig. 3. Comparison with Reocreux's test 403.

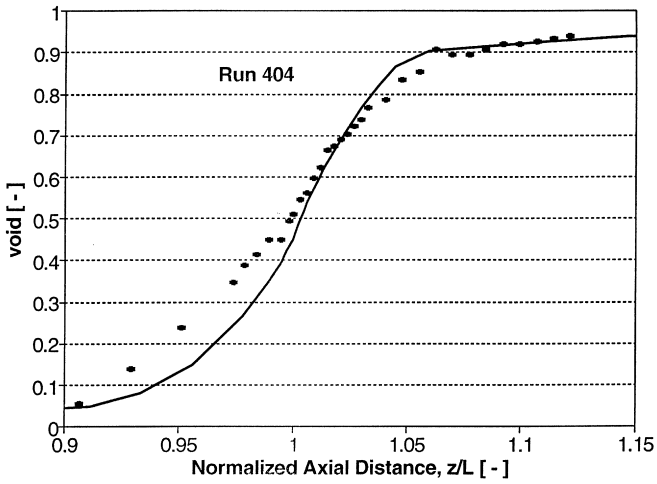

Fig. 4. Comparison with Reocreux's test 404.

section inlet is at $z/L = -0.773$. The model predictions are generally in good agrement with the measured data for the entire length of the test section.

Fig. 8 illustrates the numerical results of the vapor generation rate and the liquid degree of superheat along the tube for run ♯400 of Reocreux (1974). Both Γ and ΔT substantially increase toward the throat at $z/L = 1$ upstream of the choking plan. The void generation rate rises more gradually downstream for about 0.1 m into the diffuser section at which point both Γ and ΔT reach their maximum values and start to decrease reaching near equilibrium conditions at the exit plane.

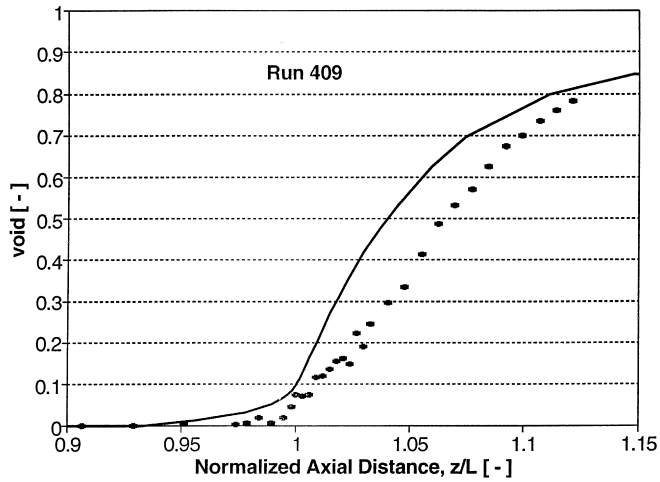

Fig. 5. Comparison with Reocreux's test 409.

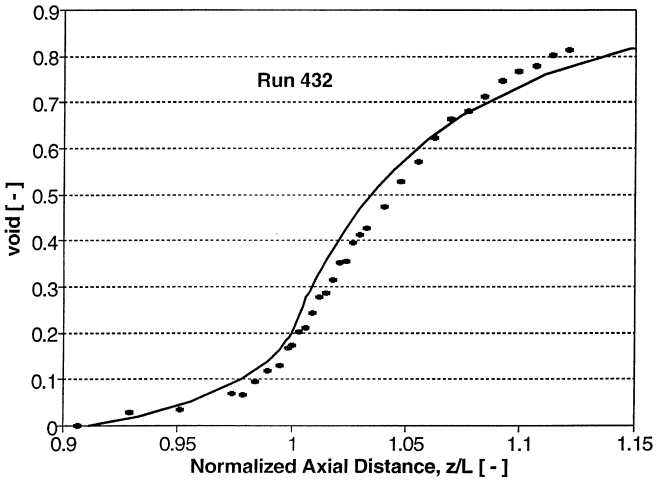

Fig. 6. Comparison with Reocreux's test 432.

5. Conclusions

A vapor species equation was applied for the analysis of flashing flows in tubes. The model accounts for both the process of explosive vapor generation at the flashing inception point and the continuous nucleation downstream, thus avoiding the usually made assumptions of constant bubble number density and uniform bubble radius. Model predictions include the thermal and transport conditions at the critical point and the details of the vapor population along the tube.

A constitutive model for the vapor generation rate is derived from the analytical solution of

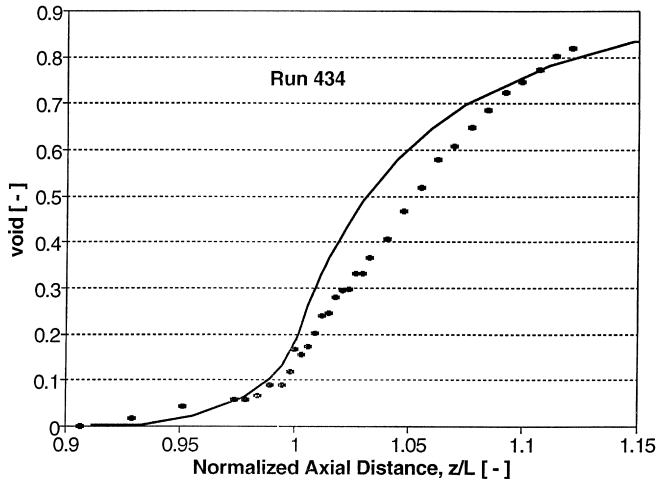

Fig. 7. Comparison with Reocreux's test 434.

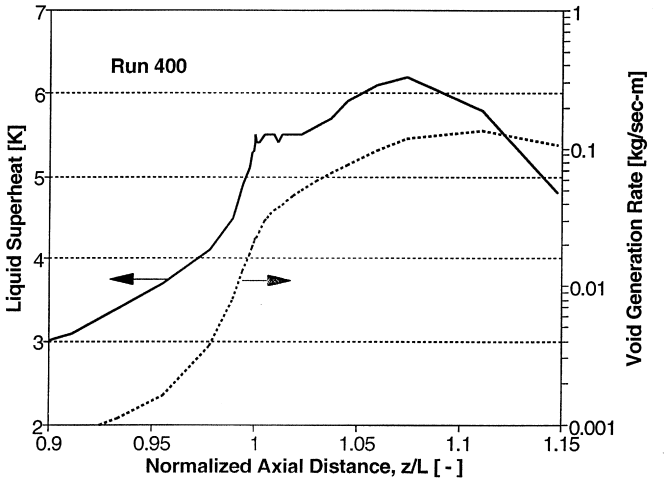

Fig. 8. Liquid superheat and void generation rate along a flow path.

the bubble species equation. The degree of thermal and mechanical nonequilibrium at the throat has a significant effect on the flow in the diffuser section. The good agreement between the predicted results and the measured void fraction in the diffuser section (Reocreux, 1974) also attests to the credibility of the present flashing model.

Acknowledgements

This research was supported by the fund for the promotion of research at the Technion.

References

Alamgir, Md, Kan, C.Y., Lienhard, J.H. 1981 Early response of pressurized hot water in a pipe to a sudden break. EPRI NP-1867.

Alamgir, Md, Lienhard, J.H., 1981. Correlation of pressure undershoot during hot water depressurization. ASME J. Heat Transfer 103, 52–55.

Ardron, K.H., 1978. A two-fluid model for critical vapor–liquid flow. Int. J. Multiphase Flow 4, 323–337.

Blander, M., 1979. Bubble nucleation in liquids. Advances in Colloid and Interface Science 10, 1–32.

Cheremisinoff, N.P., Gupta, R., 1983. Handbook of Fluid in Motion. Butterworths, Boston.

Dagan, R., Elias, E., Wacholder, E., Olek, S., 1993. A two-fluid model for critical flashing flows in pipes. Int. J. Multiphase Flow 19, 15–25.

Edwards, A.R. 1968 Conduction controlled flashing of a fluid and the prediction of critical flow rates in a one-dimensional system. AHSB Report (S), R–147.

Elias, E., Chambré, P.L., 1984. A mechanistic non-equilibrium model for two-phase critical flow. Int. J. Multiphase Flow 10, 21–40.

Elias, E., Chambré, P.L., 1993. Flashing inception in water during rapid decompression. ASME J. Heat Transfer 115, 231–238.

Elias, E., Lellouche, G.S., 1994. Two-phase critical flow. Int. J. Multiphase Flow 20 (Suppl), 91–168.

Forster, H.K., Zuber, N., 1954. Growth of a vapor bubble in a superheated liquid. J. Appl. Phys 25, 474–478.
Frenkel, J., 1955. The Kinetic Theory of Liquids. Dover Publ. Inc, New York.
Guido-Lavalle, G., Carrica, P., Clausse, A., Qazi, M.K., 1994. A bubble number density constitutive equation. Nucl. Eng. Des 152, 213–224.
Harmathy, T.Z., 1960. Velocity of large drops and bubbles in media of infinite or restricted extent. AIChE Journal 6 (2).
Herrero, V.A., Guido-Lavalle, G., Clausse, A., 1995. Non-equilibrium effects in void fraction distribution. Nucl. Eng. Des 154, 183–192.
Hirth, J.P., Pound, G.M., 1963. Condensation and Evaporation: Nucleation and Growth Kinetics. Pergamon Press, Oxford, United Kingdom.
Ishii, M., 1975. Thermo-Fluid Dynamic Theory of Two-Phase Flow. Eyrolles, Paris.
Lee, S.Y., Schrock, V.E., 1990. Critical two-phase flow in pipes for subcooled stagnation states with cavity flooding incipient flashing model. ASME J. Heat Transfer 112, 1032–1040.
Lemonnier, H., Selmer-Olsen, S., 1992. Experimental investigation and physical modeling of two-phase two-component flow in a converging-diverging nozzle. Int. J. Multiphase Flow 18, 1–20.
Minzer, U. 1995 Non-equilibrium two-phase critical flow, M.Sc. Thesis, Technion (In Hebrew).
Olek, S., Zvirin, Y., Elias, E., 1990. Bubble growth prediction by the hyperbolic and parabolic heat conduction equations. Wärme—und Stoffübertr 25, 17–26.
Reocreux, M. 1974 Contribution to the study of critical flow rates in two-phase water vapor flow. Ph.D. Thesis, Medical University of Grenoble.
Riznic, J.R., Ishii, M., 1989. Bubble number density and vapor generation in flashing flow. Int. J. Heat Mass Transfer 32, 1821–1833.
Ruggles, A.E., Lahey, R.T., Drew, D.A., Scarton, H.A., 1989. The relationship between standing waves, pressure pulse propagation, and critical flow rate in two-phase mixtures. ASME J. Heat Transfer 111, 467–473.
Saha, P., Abuaf, N., Wu, B.J.C., 1984. A non-equilibrium vapor generation model for flashing flows. ASME J. Heat Transfer 106, 198–203.
Skripov, V.P., et al., 1988. Thermophysical Properties of Liquids in the Metastable (Superheated) State. Gordon and Breach Science Publishers, New York (English Translation).
Wallis, G.B., 1969. One-Dimensional Two-Phase Flow. McGraw-Hill, New York.
Wolfert, K., 1976. The simulation of blowdown processes with consideration of thermodynamic phenomena. In: Proceedings of CSNI Meeting on Transient Two-Phase Flow 1, Toronto, 3–4 August.
Wu, B.J.C., Abuaf, N., Saha, P. 1981 A study of nonequilibrium flashing of water in a converging-diverging nozzle, NUREG/CR-1864, BNL-NUREG-51317 (June).
Yan, F. 1991 Modelisation de l'autovaporisation en écoulements subcritiques et critiques. Ph.D. Thesis, Universite Catholique de Louvain, Belgium.